Manuscript prepared for Geosci. Model Dev.
with version 2015/04/24 7.83 Copernicus papers of the LATEX class copernicus.cls.
Date: 12 September 2016

Equilibrium absorptive partitioning theory between multiple aerosol particle modes

Matthew Crooks[1], Paul Connolly[1], David Topping[1], and Gordon McFiggans[1]

[1]The School of Earth, Atmospheric and Environmental Science, The University of Manchester, Oxford Road, Manchester, M13 9PL

Correspondence to: matthew.crooks@manchester.ac.uk

Abstract. An existing equilibrium absorptive partitioning model for calculating the equilibrium gas and particle concentrations of multiple semi-volatile organics within a bulk aerosol is extended to allow for multiple involatile aerosol modes of different sizes and chemical compositions. In the bulk aerosol problem, the partitioning coefficient determines the fraction of the total concentration of semi-volatile material that is in the condensed phase of the aerosol. This work modifies this definition for multiple polydisperse aerosol modes to account for multiple condensed concentrations; one for each semi-volatile on each involatile aerosol mode. The pivotal assumption in this work is that each aerosol mode contains an involatile constituent thus overcoming the potential problem of smaller particles evaporating completely and then condensing on the larger particles to create a monodisperse aerosol at equilibrium. A parameterisation is proposed in which the coupled non-linear system of equations is approximated by a simpler set of equations obtained by setting the organic mole fraction in the partitioning coefficient to be the same across all modes. By perturbing the condensed masses about this approximate solution a correction term is derived that accounts for much of the removed complexities. This method offers a greatly increased efficiency in calculating the solution without significant loss in accuracy, thus making it suitable for inclusion in large scale models.

1 Introduction

Volatile and semi-volatile compounds are of key importance to a wide variety of industries (Biniecka and Caroli, 2011) including atmospheric science (Topping et al., 2013; Topping and McFiggans, 2012), pharmaceuticals (Sitaramaraju et al., 2008; Wang et al., 2011), food and drink (Vernocchi et al., 2008; de Roos, 2003; Hui et al., 2010; Mendes et al., 2012), water treatment (Zarra et al., 2009) and perfume (Morris, 1984). Many of these industries exploit the scented properties of a large number of semi-volatiles and an understanding of their behaviour is crucial in order to identify, produce and capture certain aromas as well as controlling the rate of their subsequent evaporation in, for example, the perfume industry. In the water treatment sector the odorous properties are not considered a favourable quality and inhibiting their release is important. The production of volatile

compounds from all of these industries, however, can have far reaching negative consequences on both health and the environment (Klein, 1995; Epstein and Gibson, 2013; Wu et al., 2009) as well as influencing weather and climate (Morgan et al., 2010).

30   This paper approaches the study of semi-volatile compounds from an atmospheric and cloud physics perspective but the equilibrium partitioning theory presented herein is applicable to the wide variety of problems outlined above. The condensed phases of the semi-volatile compounds in the atmosphere occur within aerosol particles which can have a profound effect on cloud properties and climate. The ability of an aerosol particle to act as a cloud condensation nucleus (CCN) is deter-

35   mined by many factors including size, number concentration and chemical composition, as well as the supersaturation of the air (Pruppacher and Klett, 1977). An increase in number concentration of a monodisperse aerosol which acts as a CCN will, in general, produce a greater number of smaller cloud droplets as there are more particles competing for the same available water (Twomey, 1959). In contrast, according to Köhler theory, the larger aerosol particles in a polydisperse system will

40   have a greater affinity to activate into cloud droplets and their presence can deplete the available water vapour more quickly than smaller ones, due to their quicker growth rates. Consequently, the presence of larger CCN can suppress the supersaturation causing fewer smaller particles to activate (Ghan et al., 1998).

The aforementioned effects of aerosol size and number concentration can alter precipitation rates

45   and, as a result, the lifetime of clouds (Stevens and Feingold, 2009; Albrecht, 1989). In addition to a tangible effect of an increase in number of cloud droplets leading to both an increase in reflected shortwave radiation and absorbed longwave radiation (McCormick and Ludwig, 1967; Chýlek and Coakley Jr, 1974) there is a complicated interdependency between cloud longevity and albedo (Twomey, 1974, 1977). The result is an approximate 0.7 W m^{-2} decrease in mean global

50   radiative forcing; although this is subject to a large degree of uncertainty, which is a similar order of magnitude to the mean total radiative forcing from anthropogenic activity (Forster et al., 2007; Lohmann et al., 2000).

Quantifying the size and chemical composition of individual aerosol particles within a population is complicated due to them being a heterogeneous mix of primary and secondary particles, as

55   well as secondary aerosol mass. Primary aerosol particles are emitted directly from biogenic and anthropogenic sources. Although some models exist to simulate purely semi-volatile primary particles (Tsimpidi et al., 2014) in this paper they are assumed to contain at least a small portion of non-volatile material. Secondary aerosol particles are formed by nucleation of vapours to form nanometer sized particles while secondary aerosol mass is formed by condensation of gases onto existing

60   particles. The formation of secondary aerosol mass occurs both on the primary and secondary particles and can increase the size of the secondary particles to climate-relevant sizes. The condensation process that forms secondary aerosol mass is fairly well understood for inorganic gases (Hallquist et al., 2009), however, there is significant uncertainty associated with the formation of secondary

organic aerosol (SOA) from volatile organic compounds (VOCs). Part of this uncertainty is a result of the poorly quantified process of oxidation of VOCs to produce SOA and other VOCs with reduced volatility (Jimenez and et. al., 2009; Yu, 2011).

Over remote continental regions between 5% and 90% of the total aerosol mass can be made up of organic material (Andreae and Crutzen, 1997; Zhang et. al., 2007; Gray et al., 1986) and a significant proportion of this can be from secondary sources. SOA in such large quantities will act to increase the size of the particles as well as significantly changing their chemical composition. The effect of the increased size, and consequently soluble mass, is found to be the dominant effect on cloud; increasing the number of cloud droplets and subsequently decreasing the critical supersaturation (Dusek et al., 2006; Topping et al., 2013).

It is estimated that $10^4 - 10^5$ organic species have been measured in the atmosphere but this may only be a small proportion of the total (Goldstein and Galbally, 2007). Of this number fewer than 3000 have actually been identified (Simpson et al., 2012; Borbon et al., 2013). It is, therefore, impractical to try to model each compound individually. Instead, fewer surrogate species are used to represent many different compounds. O'Donnell et al. (2011), for example, uses α-pinene as a surrogate for all monoterpenes and xylene to represent multiple aromatic compounds.

Two popular methods have been developed to simulate multiple organic species using equilibrium absorptive partitioning theory (Pankow, 1994); a method of calculating the equilibrium condensed concentrations without solving the computationally expensive dynamic condensation and evaporation processes. The first (Odum et al., 1996) involves an empirically fitted relation derived from two-compound experiments which benefits from its simplicity but, as with any empirical relation, has possibly limited applicability outside of the original constraints. In particular, the approach has been found to be unrealistically sensitive to changes in concentration of the organics (Cappa and Jimenez, 2010). The second (Donahue et al., 2006) uses a volatility basis set; binning large numbers of semi-volatile organic compounds (SVOCs) into a small number of representative species with effective saturation concentrations. This method was later extended to account for partitioning of both water and SVOCs (Barley et al., 2009) by treating the water as an additional volatile substance.

A limitation of equilibrium absorptive partitioning theory (Pankow, 1994) is the assumption of well mixed particles. Although some experimental results indicate that aerosol particles containing SOA can exist in highly viscous states (Vaden et al., 2011; Cappa and Wilson, 2011), it is still an active area of research especially in relation to high relative humidities and the effects on cloud droplet formation. Numerical models investigating the effect of diffusion within aerosol particles (Zobrist et al., 2011; Smith et al., 2003) indicate a transition from a glassy to a liquid phase of the particles above about 50% relative humidity, which is often encountered in the atmosphere and is of particular relevance in cloud microphysics.

The focus of this paper is on the condensation of SVOCs within the atmosphere and we assume that there are sufficient aerosol particles that the process of condensation onto existing particles is the

dominant sink for the SVOCs over nucleation of new particles. We also assume that existing particles, which act as a seed for the condensation, are involatile although in many applications particles that have previously nucleated from oxidation of extremely low volatility compounds can also be approximated as being involatile (Ehn et al., 2014). Consequently, every particle considered in this paper is assumed to have at least a small portion of an involatile compound which cannot evaporate into the vapour phase. This assumption is crucial in calculating the equilibrium vapour/condensed phases on multiple modes as without it, a polydisperse equilibrium does not exist. In the purely volatile particle case, the smaller particles evaporate completely thus allowing the larger particles to take up additional condensed mass to produce a monodisperse aerosol at equilibrium.

In this paper we present a model for equilibrium absorptive partitioning of water and SVOCs onto multiple involatile aerosol modes using the volatility basis set method of Donahue et al. (2006). All compounds are considered to be at least partially soluble so that the involatile aerosol influences the partitioning of the SVOCs and the particles are assumed to be always well mixed. The concentration of a SVOC in the condensed phase on one mode has the effect of reducing the total concentration available to the other modes and as a result, the equilibrium vapour/condensed phases of all the organics on all the involatile modes must be solved for simultaneously. By assuming all modes have approximately the same organic mole fraction, a parameterisation for the solution is derived that has a high degree of accuracy while being significantly more efficient than a standard numerical algorithm would be. Condensed concentrations of organics are compared against equilibrium calculated from a dynamic condensation model and are found be comparable.

2 Equilibrium Absorptive Partitioning Theory for Size Independent Bulk Aerosol

Before introducing the new multiple mode equilibrium partitioning theory, we first review existing partitioning theories, beginning with that for a bulk aerosol. The volatility basis set of Donahue et al. (2006) involves binning multiple organic species into groups of compounds with similar saturation concentrations, $\mathcal{C}_j^*$. Each volatility bin is then represented by a single representative species with an effective $\mathcal{C}_j^*$ value. A $\log_{10}$ volatility basis set is used with $\mathcal{C}_j^*$ values from $1 \times 10^{-6} \mu$g m^{-3} to $1 \times 10^3 \mu$g m^{-3} (Cappa and Jimenez, 2010; Donahue et al., 2006). We use the notation, $\mathcal{C}_j^*$, for the saturation concentration measured in μg m^{-3} to distinguish from the analogous molar quantity (Barley et al., 2009), C_j^*, in units of μmol m^{-3} obtained by dividing $\mathcal{C}_j^*$ by the molecular weight. The value of C_j^* is proportional to the saturation vapour pressure, p_j^o (atm), of the organics in the jth volatility bin at temperature, T_0, through the equation

$$C_j^* = \frac{p_j^o \gamma_j 10^6}{R T_0}.$$ (1)

Here γ_j is the the activity coefficient of the organics in the jth bin, R is the universal gas constant (m^3 atm mol^{-1}K^{-1}) and T_0 is the temperature (K). The saturation vapour pressure is dependent on the temperature, T_0, which is taken to be 298.15K. Conversion to a C^* at another temperature, T,

can be done using the Clausius Clapeyron equation,

$$C^*(T) = C^*(T_0)\frac{T_0}{T}exp\left[-\frac{\Delta H_{vap}}{R}\left(\frac{1}{T}-\frac{1}{T_0}\right)\right],$$

where ΔH_{vap} is the enthalpy of vapourisation of the organic compounds and is taken to be 150 kJ mol^{-1} in the current work.

140   Water and other inorganic semi-volatile compounds can additionally be considered by binning them along with the organics. For simplicity we ignore inorganic semi-volatiles and for the purposes of applying the theory to the particular problem of cloud physics later in the paper we treat water as a separate volatile compound so that its abundance can be varied independently of the organics.

The total concentration of the SVOCs in the jth volatility bin is defined by C_j (μ mol m^{-3}) and

145   is decomposed into a vapour and a condensed phase,

$$C_j = C_j^v + C_j^c, \tag{2}$$

indicated by the superposed v and c respectively. The total concentration of all compounds in the condensed phase, C_T, is the sum of the concentration of ions of involatile aerosol, C^o, the condensed water, C^w, and each organic component in the condensed phase,

150    $$C_T = C^o + C^w + \sum_k C_k^c. \tag{3}$$

The condensed water can be calculated assuming ideality by equating the saturation ratio, S, to the mole fraction of water,

$$S = \frac{C^w}{C^o + C^w + \sum_k C_k^c}. \tag{4}$$

Equation (4) can be rearranged to make C^w the subject and then substituted into (3) and factorised

155   to give

$$C_T = \frac{1}{1-S}\left(C^o + \sum_k C_k^c\right). \tag{5}$$

The analogous expression to (4) for the organics is

$$\frac{C_j^v}{C_j^*} = \frac{C_j^c}{C_T}, \tag{6}$$

where the saturation ratio has been replaced by the ratio of the vapour pressure to the saturation

160   vapour pressure of the jth component using (1).

Eliminating C_j^v from (2) using (6) and rearranging gives the condensed concentration of the jth organic component in terms of the total concentration

$$C_j^c = C_j\left(1 + \frac{C_j^*}{C_T}\right)^{-1}. \tag{7}$$

The partitioning coefficient is defined as

165    $$\xi_j = \left(1 + \frac{C_j^*}{C_T}\right)^{-1}, \tag{8}$$

so that $C_j^c = \xi_j C_j$. Since C_T depends on the C_j^c this problem must be solved iteratively; calculating the C_j^c given an initial C_T, using these values to update the value of C_T and repeating until equation (5) is satisfied within some tolerance.

3 Equilibrium Absorptive Partitioning Theory for a Monodisperse Aerosol

170 The theory in the previous section is independent of the size of the aerosol particles. We extend this theory to include size dependence for a monodisperse aerosol. The partitioning of water is influenced by the size of the aerosol particles through the Kelvin factor,

$$K^w = \exp\left(\frac{4M_w\sigma}{\rho_w RTD}\right),$$

where M_w, ρ_w and σ are the molecular weight, density and surface tension of water, and D is the

175 diameter of the wet aerosol particles. The Kelvin factor multiplies the right-hand side of equation (4), see, for example, Rogers and Yau (1996),

$$S = \frac{C^w K^w}{C^o + C^w + \sum_k C_k^c}. \tag{9}$$

Consequently, the right hand side of equation (5) becomes

$$C_T = \frac{K^w}{K^w - S}\left(C^o + \sum_k C_k^c\right), \tag{10}$$

180 and for notational simplicity we define the prefactor on the right-hand side by η,

$$\eta = \frac{K^w}{K^w - S}.$$

The Kelvin factor for the organics, K_j, is defined by Cai (2005) as

$$K_j = \exp\left(\frac{4M_j\sigma}{\rho_j RTD}\right), \tag{11}$$

where M_j and ρ_j are the molecular weight and density of the organics in the jth volatility bin, and

185 σ is the surface tension of the particle with condensed organics and water. This is included into equation (6) in an analogous way to the Kelvin factor for water to give

$$\frac{C_j^v}{C_j^*} = \frac{C_j^c K_j}{C_T}, \tag{12}$$

and consequently the partitioning coefficient is defined as

$$\xi_j = \left(1 + \frac{C_j^* K_j}{C_T}\right)^{-1}. \tag{13}$$

190 This set of algebraic equations again needs to be solved iteratively as in the previous section but with the addition of calculating the diameter, and consequently Kelvin term, from the C_j^c at each iteration.

4   Equilibrium Absorptive Partitioning Theory for a Conglomeration of Particles of Multiple Sizes and Composition

An aerosol population commonly comprises particles of different sizes and chemical composition. In this section we consider aerosol which can be decomposed into multiple monodisperse aerosol modes. We propose a novel extension to the theory of the previous sections which is applicable to these more diverse conglomerations of particles and therefore suitable for application to a wider class of problems.

The most significant change to the theory for multiple modes is that the equations must explicitly take into account that a single molecule of an organic cannot condense onto more than one mode. Consider the 10 organic molecules and 2 involatile particles shown in blue and green respectively in Figure 1. Suppose the subset highlighted in pink are known to condense onto the left involatile particle; these molecules cannot also condense onto the right particle. Hence, the only molecules available to condense onto the right particle are those circled by the dashed line. The converse is also true; if the molecules highlighted in pink in Figure 2 are known to condense onto the right particle then only the remaining molecules are free to condense onto the left particle. As such, the concentration of organics in the jth volatility bin which is available to the ith mode is the total concentration in the jth volatility bin minus the condensed concentrations of the organics in the jth bin on the other modes. It is this remaining vapour phase that is multiplied by the partitioning coefficient in the multiple mode case.
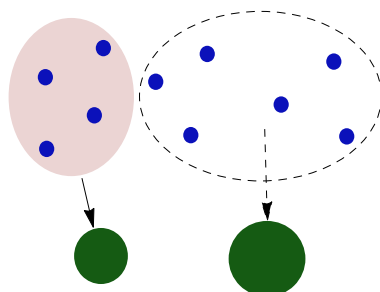
Figure 1. A representation of the condensation of a SVOC, shown by the blue dots, onto two non-volatile particles, shown by the green circles. The SVOC is divided into two groups; those that condense onto the left involatile particle (highlighted in pink) and those remaining to equilibrate on the right particle (circled by the dashed black line).

We make the following changes to extend the theory in the previous section to the multiple mode case:

- The condensed mass of the jth organic component will now be split across several modes. Define the condensed concentration of the jth organic species on the ith involatile mode by
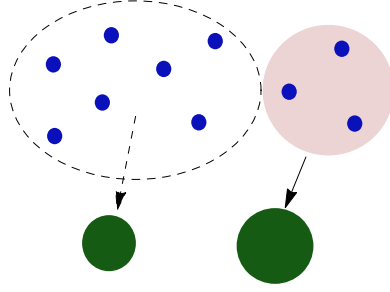
Figure 2. Same as Figure 1 but with the known number of molecules (highlighted in pink) on the second mode.

C_{ij}^c so that the condensed phase C_j^c can we expressed as the sum

$$C_j^c = \sum_r C_{rj}^c. \tag{14}$$

For consistency, a subscript i refers to the involatile mode and j refers to the jth volatility bin. Separate indices r and k are used in the summations to make clear which terms are being summed and are applied to summations over i and j, respectively. Subsequently, the total concentration of semi-volatiles in the jth volatility bin is decomposed into a single vapour phase and the sum of the multiple condensed phases

$$C_j = C_j^v + \sum_r C_{rj}^c. \tag{15}$$

The total concentration in the condensed phase on the ith mode is given by the sum of the concentrations of the involatile constituent and all of the condensed organics and water on the ith mode,

$$C_{T,i} = C_i^o + C_i^w + \sum_k C_{ik}^c,$$

which can equally be expressed in an analogous way to (10) as

$$C_{T,i} = \frac{K_i^w}{K_i^w - S} \left(C_i^o + \sum_k C_{ik}^c \right). \tag{16}$$

Here

$$K_i^w = \exp\left(\frac{4M_w\sigma}{\rho_w RTD_i} \right),$$

is the Kelvin factor of water and C_i^o is the number of μmol per cubic meter of the ith involatile aerosol mode. D_i is the diameter of the ith mode with both condensed water and organics. For

notational simplicity we define

$$\eta_i = \frac{K_i^w}{K_i^w - S}, \tag{17}$$

so that (16) can be written as

$$C_{T,i} = \eta_i \left(C_i^o + \sum_k C_{ik}^c \right). \tag{18}$$

– The partitioning coefficient, given by (13), depends on the material properties and size of the involatile aerosol particles, through C_T and K_j, and consequently each volatility bin can have a different coefficient for each mode. The Kelvin factor for the jth volatility bin, (11), is modified to depend on the diameter of the ith composite mode, D_i,

$$K_{ij} = \exp \left(\frac{4M_j \sigma}{\rho_j R T D_i} \right),$$

Subsequently, the multiple mode analogy to (12) on the ith mode is

$$\frac{C_j^v}{C_j^*} = \frac{C_{ij}^c K_{ij}}{C_{T,i}}, \tag{19}$$

This can be used to eliminate the vapour concentration from (15)

$$C_j = \frac{C_j^* C_{ij}^c K_{ij}}{C_{T,i}} + \sum_r C_{rj}^c. \tag{20}$$

The concentration C_{ij}^c can be extracted from the sum on the right-hand side and the equation rearranged to give

$$C_j - \sum_{r \neq i} C_{rj}^c = C_{ij}^c \left(1 + \frac{C_j^* K_{ij}}{C_{T,i}} \right). \tag{20}$$

We denote the partitioning coefficient for the jth organic component onto the ith involatile mode by ξ_{ij} and define it in an analogous way to (13),

$$\xi_{ij} = \left(1 + \frac{C_j^* K_{ij}}{C_{T,i}} \right)^{-1}. \tag{21}$$

– The total concentration of the jth organic which is available to the ith involatile mode, as previously discussed, can now be defined

$$C_{ij} = C_j - \sum_{r \neq i} C_{rj}^c,$$

or alternatively

$$C_{ij} = C_j - \sum_r C_{rj}^c + C_{ij}^c. \tag{22}$$

– An expression for the condensed concentration of the jth organic on the ith involatile mode can now be expressed as the product of the partitioning coefficient with C_{ij},

$$C_{ij}^c \quad = \quad \frac{C_j - \displaystyle\sum_r C_{rj}^c + C_{ij}^c}{1 + \dfrac{C_j^* K_{ij}}{C_{T,i}}}, \tag{23}$$

which is a rearrangement of (20). Replacing $C_{T,i}$ using (18) yields

$$C_{ij}^c \quad = \quad \frac{C_j - \displaystyle\sum_r C_{rj}^c + C_{ij}^c}{1 + \dfrac{C_j^* K_{ij}/\eta_i}{C_i^o + \displaystyle\sum_k C_{ik}^c}}. \tag{24}$$

The non-linear nature of these equations poses a problem for obtaining a solution. Numerical methods exist for solving such problems, but require an initial guess for the solution. Furthermore, there are multiple unknowns and multi-dimensional non-linear solvers are too computationally expensive to implement in a global climate model. In the following section, we present a method for obtaining an approximate solution to the system of equations represented by (24) which facilitates a numerical solver in computing the full solution. This approximation, however, is found to be sufficiently accurate that an analytic perturbation method, derived in Section 5.4, can be used to reduce the inaccuracies and render the costly numerical solution redundant.

5 A parameterisation for the condensed concentrations

We present in this section a proposed parameterisation to calculate the condensed concentrations of SVOCs that approximates the solution to the multiple mode equilibrium absorptive partitioning equations represented by (24). We begin by simplifying the equations assuming that all modes share a common average organic mole fraction and the resulting equations are derived in Section 5.2. This approximation can either be used as an initial condition for a numerical algorithm to solve the full system of equations represented by (24) or, as we suggest in Section 5.4, can be used as a leading order solution in a perturbation method in order to derive a correction term that reintroduces much of the removed complexities. We begin by justifying the assumption of the common organic mole fraction.

5.1 Motivation

To demonstrate that the individual organic mole fractions of the different modes are comparable we have run a Monte Carlo simulation that solves the system of equations represented by (24) for

randomly chosen parameter values taken from Table 1. Low accuracy solutions of (24) for the equilibrium concentrations in the condensed phase are found using a brute force trial and error method. 50 such solutions for between 2 and 5 involatile modes are shown in Figure 3 with each calculated using different randomised parameter values. The concentrations of organics in each volatility bin are kept in the proportions shown in Table 2 but are rescaled by a random factor of between 0 and 100. Plotted in the graph is the organic mole fraction that we define as the total concentration of semi-volatile material on a mode divided by the total number of ions in the aerosol. For the ith mode this is

$$\theta_i = \frac{\sum\limits_k C_{ik}^c}{C_i^o + \sum\limits_k C_{ik}^c},$$ (25)

Each solution is represented by several dots joined by a vertical line with the y coordinate of the dots showing the mole fraction of one of the modes. These are plotted against the average mole fraction of all the modes in that solution on the x axis. As can be seen from Figure 3, even though the mole fractions are different, they never deviate too far from the mean, shown by the dashed line. Assuming the same mole fraction for all the modes allows approximate values of $C_{T,i}$ to be found in terms of a single parameter. This greatly simplifies the problem and can provide a reasonable guess for the non-linear solver.

We emphasise that although the mole fractions of the different modes are comparable, the equilibrium partitioning solution is still dependent on the individual material properties of the involatile aerosol with number concentration, size, molecular weight, density and van't Hoff factors all influencing the number of moles of the involatile compound and consequently the number of moles of condensed organics required to give the appropriate mole fraction.

Table 1. Randomised parameters used to plot Figure 3. N_i, D_i, ρ_i^o and M_i^o are the number concentration, diameter, density and molecular weight of the ith involatile aerosol, respectively. ν_i^o and ν_j are the van't Hoff factors of the involatile constituents and organics.

parameter	N_i (cm^{-3})	D_i (nm)	ρ_i^o (kg m^{-3})	ρ_i (kg m^{-3})	M_j, M_i^o (kg mol^{-1})	ν_i^o	ν_j
min	50	50	500	500	0.1	1	0
max	500	500	2000	1500	0.4	3	1

5.2   Derivation of a solution with a common average organic mole fraction

The previous section showed that the organic mole fraction of individual modes is always similar to the mean organic mole fraction across all modes. By making the assumption of a common mole fraction, we now derive a new set of equations to calculate approximate condensed concentrations of the SVOCs that contain only one unknown in the denominators of the partitioning coefficients.
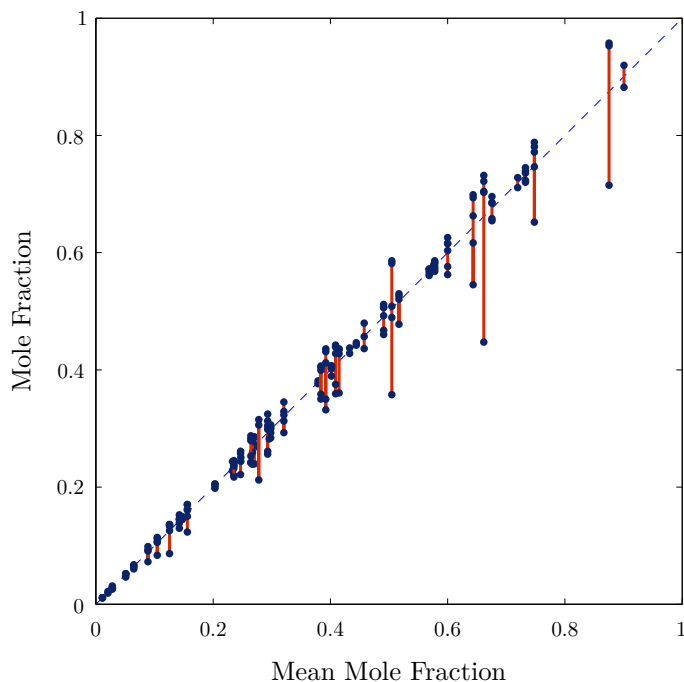
Figure 3. The mole fractions of multiple different involatile aerosol modes plotted against mean mole fraction on the x axis. 50 solutions are shown with parameters randomly chosen from the ranges shown in Table 1 with $RH = 0\%$. The volatility distribution of SVOCs is shown in Table 2 but are rescaled by a random factor of between 0 and 100.

310   Using a root-finder algorithm the common mole fraction can be iterated until it is equal to the mean organic mole fraction across all modes.

     The solution derived under the assumption of a common mole fraction, θ, is referred to as the leading order solution and is denoted, $\bar{C}_{ij}^c$. Rearranging (25) with θ_i replaced by θ gives

$$\frac{\theta}{1-\theta} = \frac{\sum\limits_{k} \bar{C}_{ik}^c}{C_i^o}. \tag{26}$$

315   The left-hand side of this equation is the same for all the modes and consequently the right-hand side must also be the same. For notational simplicity we combine the left-hand side into a single parameter, β,

$$\beta = \frac{\theta}{1-\theta} = \frac{\sum\limits_{k} \bar{C}_{ik}^c}{C_i^o}, \tag{27}$$

and subsequently

320    $$\sum_{k} \bar{C}_{ik}^c = \beta C_i^o. \tag{28}$$

     The wet diameter of the combined aerosol is assumed to be sufficiently large that the Kelvin factors for the SVOCs can be approximated by 1. The same is not true for the Kelvin factors for

water, K_i^w. If these are assumed to take the value 1 then the definition of η_i, as given by (17), will lead to a gross over estimate of the condensed water close to cloud base, becoming infinite as the relative humidity becomes 100%.

The governing equations for the leading order solution are obtained by making the approximation given by (28) together with setting $K_{ij} = 1$,

$$\bar{C}_{ij}^c = \frac{C_j - \sum_r \bar{C}_{rj}^c + \bar{C}_{ij}^c}{1 + \dfrac{C_j^*/\eta_i}{C_i^o(1+\beta)}}. \tag{29}$$

The interdependence of the $\bar{C}_{ij}^c$ can be eliminated to obtain an explicit expression for each in terms of the mole fraction β,

$$\bar{C}_{ij}^c = \frac{C_i^o(1+\beta)\left(1 - \phi_j(\beta, \eta_i)\right) C_j}{C_j^*/\eta_i}, \tag{30}$$

the algebra of this step is given in Appendix A. The dependence of ϕ_j, given by (A2), is expressed explicitly for clarity. Both sets of equations are equivalent to one another and either can be used to find the $\bar{C}_{ij}^c$. The coupled nature of equations (29), however, requires a matrix inversion to solve and this will take more time to calculate than the solution to equations (30).

The complexity of the summation of $\bar{C}_{ij}^c$ in the denominator has now been removed in favour of a single parameter, β. This can be solved for using a much quicker one-dimensional root find algorithm which iterates the value of θ; calculating β using (27) and solving the linear system of equations at each step to find $\bar{C}_{ij}^c$. The value of θ can be updated at each iteration based on the average value obtained through equation (26), namely

$$\theta = \frac{1}{n} \sum_r \left(\frac{\sum_k \bar{C}_{rk}^c}{C_r^o + \sum_k \bar{C}_{rk}^c} \right),$$

where n is the number of modes.

While the dependence of η_i on $\bar{C}_{ij}^c$ has not been removed, it is sufficiently weak that the values of $\bar{C}_{ij}^c$ calculated at the previous iteration of θ can be used to evaluate the Kelvin factor for water and therefore η_i; simultaneously converging on the correct value as θ is found.

5.3 Results

The leading order solution given in the previous section is calculated and used as an initial guess for solver of the full non-linear problem; a comparison of the two solutions are presented here. In order to test the theory over a large parameter space, values of the inputs are chosen from Table 1 and the models are run for between 2 and 6 modes. Solutions from only one mode are plotted for each run to avoid a bias towards the solutions for 6 mode runs which would otherwise have three times as many points plotted as the 2 mode runs. Concentrations of the SVOCs are chosen randomly by rescaling the volatility distribution given in Table 2 by between 0 and 100.

Table 2. Volatility distribution of SVOCs.

$\log \mathcal{C}^*$	-6	-5	-4	-3	-2	-1	0	1	2	3
$\mathcal{C}_j\ (\mu\text{g m}^{-3})$	0.005	0.01	0.02	0.03	0.06	0.08	0.16	0.3	0.42	0.8
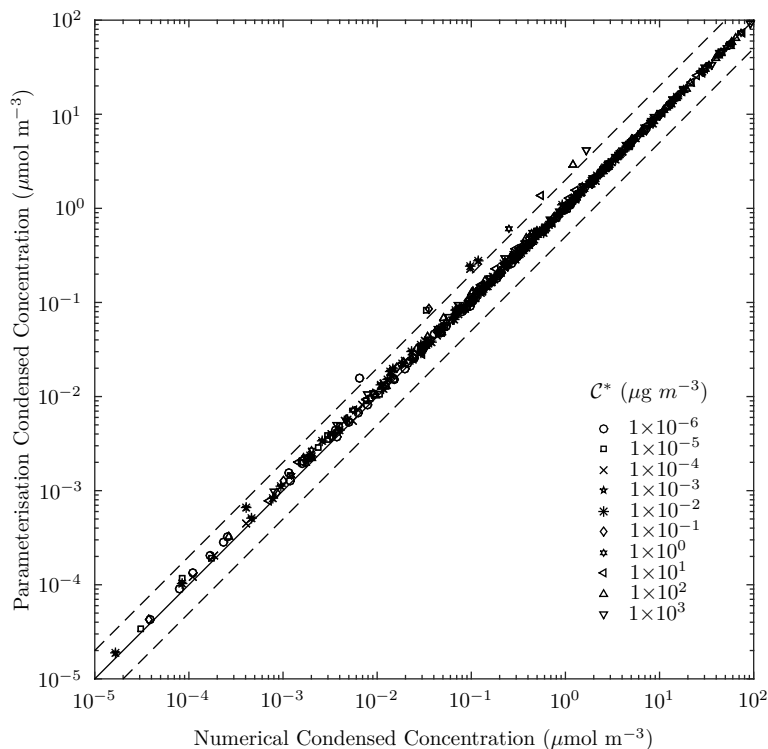
Figure 4. Comparison of the condensed concentrations of organics from the leading order solution against those calculated using the non-linear solver for randomly chosen parameters from Table 1. Concentrations of the SVOCs are chosen randomly by rescaling the volatility distribution given in Table 2 by between 0 and 100. The solution is calculated for between 2 and 6 modes and only the condensed concentrations on the first mode are plotted. The different volatility bins are distinguished by the shape of the points and the corresponding $\mathcal{C}^*$ values given in the legend. The 1:1 line is shown in solid black and the dashed lines show 1:2 and 2:1 lines.

Figure 4 shows the individual condensed masses of the 10 volatility bins, each with different shaped points. The solid black line shows equality between the approximation and the full solution and the dashed lines show 50% inaccuracies in the approximations. The very strong correlation between the full non-linear solution and the leading order solution demonstrates that the assumption of a common average organic mole fraction made in the previous section not only offers an efficient way of calculating an initial guess for the non-linear solver but actually offers an accurate approximation to the solution for the condensed masses of the organics.

Figure 5 compares the organic mass fractions, defined as the total mass of condensed organics divided by the total mass of the aerosol, from the full non-linear solution and the leading order solution from the different runs. A range of relative humidities and van't Hoff factors of the involatile aerosol are used; these values are shown above each plot. Small values of the van't Hoff factor appear to have a significant effect on the mass fraction as the correlation of the right-hand three plots is worse than the left three. This is caused by the need to divide by the van't Hoff factor when converting from number of ions to mass. The result is a high sensitivity of the mass to slight inaccuracies in the number of ions for van't Hoff factors close to zero; this is addressed in Section 5.4.

Similarly, lower values of the relative humidity reduce the correlation of the two solutions with almost perfect agreement in the lower two plots for $RH = 99.999\%$. This is likely a result of higher relative humidities increasing the wet diameter of the droplets and subsequently reducing the Kelvin factor closer to 1. Since the leading order solution sets the Kelvin factors of the organics to 1, higher values of RH improve this approximation. At $RH = 99.999\%$ the increased water content of the wet aerosol will further act to increase the value of C_T and subsequently lead to a significantly higher proportion of the organics being in the condensed phase. With nearly all the organics in the condensed phase there is much less potential for errors in the approximation.

5.4 Perturbation Solution

Although the condensed masses computed using the approximation derived in Section 5.2 did not completely agree with the full non-linear solution, the errors were small relative to the size of the C_{ij}. We propose a correction term to this approximation which improves the accuracy and also takes into account the Kelvin terms. Suppose the actual condensed masses, C_{ij}^c, can be obtained from the leading order solution, $\bar{C}_{ij}^c$, by adding a small perturbation

$$C_{ij}^c = \bar{C}_{ij}^c + \hat{C}_{ij}^c,$$

where we assume $|\hat{C}_{ij}^c| \ll |\bar{C}_{ij}^c|$. The Kelvin factors also depend on the final condensed mass and for clarity ought to be written $K_{ij} = K_{ij}(C_{ij}^c)$. This, however, adds much complexity. Therefore, it is assumed that the leading order solution provides a suitably accurate approximation to the condensed masses of semi-volatiles for the purposes of calculating the Kelvin factors. Consequently, we make the additional approximation $K_{ij}(C_{ij}^c) \approx K_{ij}(\bar{C}_{ij}^c)$ which we denote $\bar{K}_{ij}$. Similarly, $K^w(C_{ij}^c) \approx K^w(\bar{C}_{ij}^c)$ and consequently $\eta_i(C_{ij}^c) \approx \eta_i(\bar{C}_{ij}^c) = \bar{\eta}_i$. We substitute the perturbation into the equations represented by (24) together with these approximations to give

$$\bar{C}_{ij}^c + \hat{C}_{ij}^c = \frac{C_j - \sum_r \bar{C}_{rj}^c + \bar{C}_{ij}^c - \sum_r \hat{C}_{rj}^c + \hat{C}_{ij}^c}{1 + \dfrac{C_j^* \bar{K}_{ij}/\bar{\eta}_i}{C_i^o + \sum_k \bar{C}_{ik}^c + \sum_k \hat{C}_{ik}^c}}. \tag{31}$$
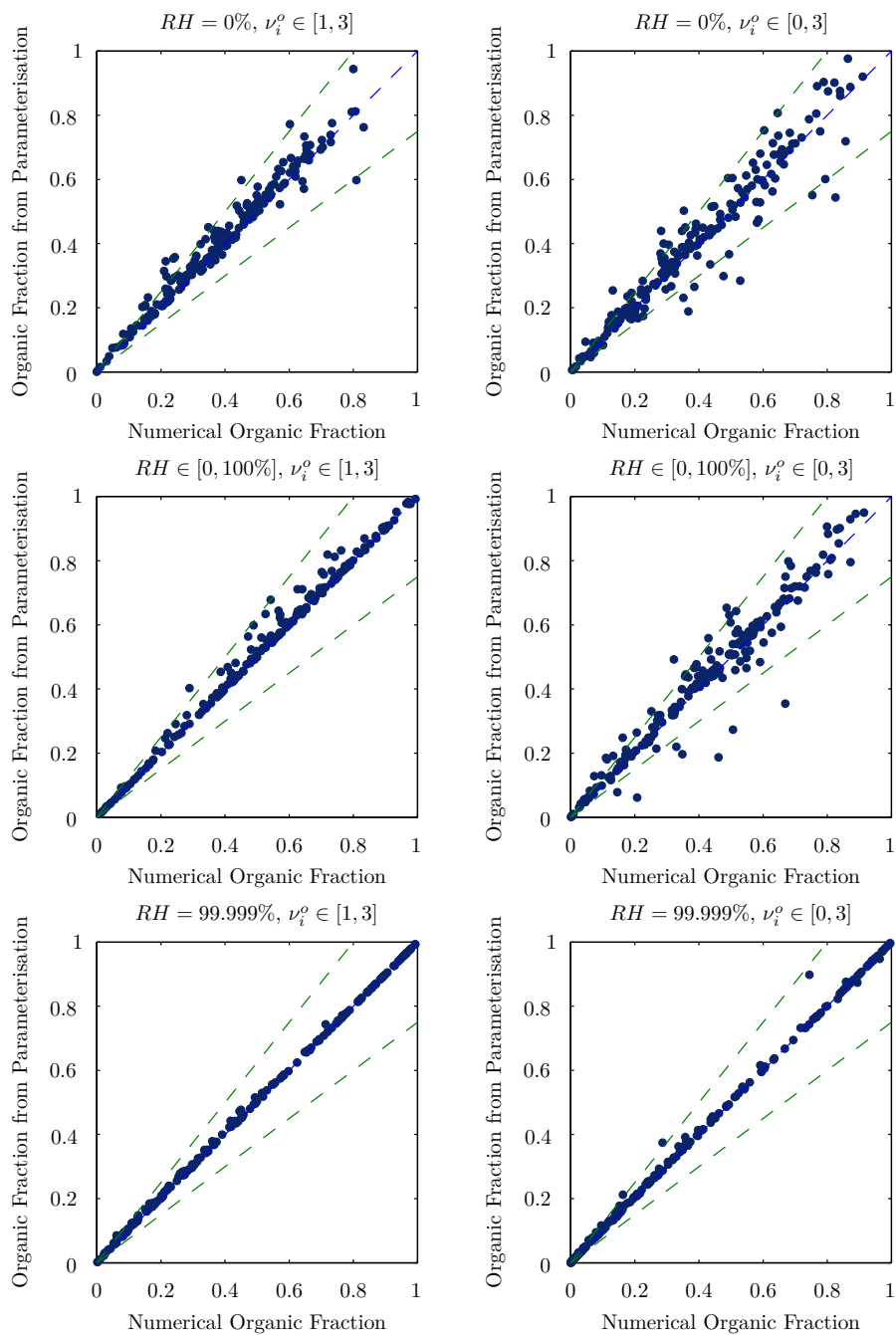
Figure 5. Comparison of the organic mass fraction from the leading order solution against that calculated using the non-linear solver for randomly chosen parameters from Table 1. SVOC concentrations are obtained by randomly rescaling the volatility distribution in Table 2 by a random factor between 0 and 100. The solution is calculated for between 2 and 6 modes and only the organic mass fraction of the first mode is plotted. 25% error margins are shown by the dashed green lines.

Assuming the perturbed quantities, $\hat{C}_{ij}^c$, are small we can linearise these equations to give

$$\left(1 - \bar{\xi}_{ij}\right)\hat{C}_{ij}^c + \bar{\xi}_{ij}\sum_r \hat{C}_{rk}^c - \mathcal{L}_{ij}\sum_k \hat{C}_{ij}^c = \frac{C_j - \sum\limits_r \bar{C}_{rj}^c + \bar{C}_{ij}^c}{1 + \dfrac{C_j^* \bar{K}_{ij}/\bar{\eta}_i}{C_i^o + \sum\limits_k \bar{C}_{ik}^c}} - \bar{C}_{ij}^c. \tag{32}$$

the algebra for which is given in Appendix B. The $\bar{\xi}_{ij}$ are the partitioning coefficients, (21), calculated using the leading order solution; explicit expressions are given by (B2). The $\mathcal{L}_{ij}$ are defined in Appendix B and are coefficients that depend on the $\bar{C}_{ij}^c$ as well as the parameters of the problem but are independent of the perturbations. Therefore, these equations are linear in the perturbations and can be solved much quicker than the full set of non-linear equations.

If the leading order solution, $\bar{C}_{ij}^c$, were the exact answer then the right-hand side would be simple a rearrangement of the equations (24) and would be zero. In such a situation, the left-hand side would also have to be zero resulting in a homogeneous system of coupled linear equations with only the trivial solution in which $\hat{C}_{ij}^c = 0$. However, the leading order solution does not satisfy the full system of equations but is "close" by some measure. Consequently, the right-hand side of (32) is "small" and defines the size of the small perturbation $\hat{C}_{ij}^c$. The additional correction term can be calculated by a simple matrix inversion owing to the linear nature of equations (32) which, as we shall see in the following section, produces a much more accurate solution in a fraction of the time it would take to run the non-linear solver.

5.5 Results

Figure 6 is a replica of Figure 4 with the addition of the condensed concentrations calculated using the first order correction term shown in red. The perturbation solution can be seen to offer an improved approximation to the leading order solution with almost perfect agreement with the non-linear solution for all concentrations.

The organic mass fractions calculated from the perturbation solution are plotted against those calculated using the non-linear solver in Figure 7 and are shown in red. The graphs show a marked improvement on the leading order solution, which are shown in navy, across all parameter space. Adding the first order correction term reduces the errors to less than 20% in the worst cases of the top right plot compared to nearly 50% in the leading order solution. The general trends of worse correlation for low RH and ν_i^o observed in Figure 5 are replicated in the perturbation solution but to a much lesser extent. This is due to the inclusion of a leading order Kelvin factor for the organics that reduces the influence of the RH and improvements in the accuracy of the condensed concentrations reduce the subsequent errors in the masses.

Figure 8 shows the percentage errors in the calculated mass fractions when compared to the solution from the non-linear solver. The top two plots, which had the worst correlation in Figure 7, show
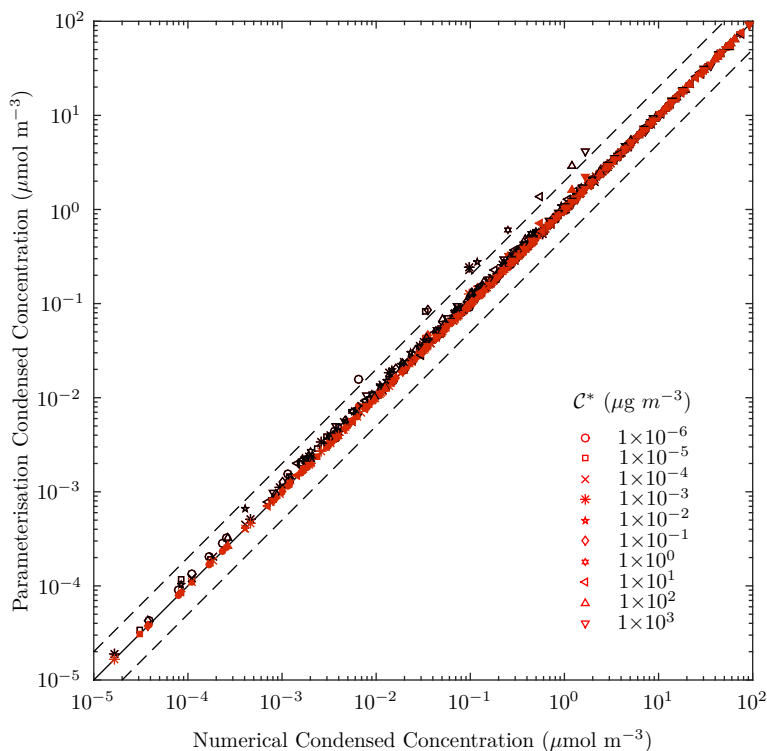
Figure 6. Same as Figure 4 with the addition of the perturbation solution shown in red.

that the leading order solution produces errors in the organic mass fraction of below 20% in nearly all cases and these reduce to 10% when the correction term in the perturbation solution is included. The affect of van't Hoff factors close to zero is most notable in the middle two plots where the errors increase about 3 fold compared to when the van't Hoff factors are greater than 1; middle right and

430 left plots, respectively. The errors in the perturbation solution rarely exceed 10% across the entire parameter space and are only a few percent at cloud base, shown by the lower 2 plots.

6 Comparison between the partitioning theory and a dynamic condensation model

The equilibrium absorptive partitioning theory presented in the previous sections calculates the equilibrium condensed concentration of each organic compound. If a dynamic model of condensation of

435 SVOCs is left to run for long enough it ought to equilibrate on the same solution. We test this in Section 6.1 for two modes as verification of the extension of the partitioning theory to multiple modes. Once we have confirmed that the dynamic model converges on the equilibrium absorptive partitioning theory solution for monodisperse modes, we investigate the performance of equilibrium partitioning theory when applied to aerosol modes that are represented by lognormal size distributions in

440 Section 6.2, which is more applicable to atmospheric models. Again, a dynamic condensation model is allowed to run until it reaches equilibrium and this solution is compared to the analogous solution
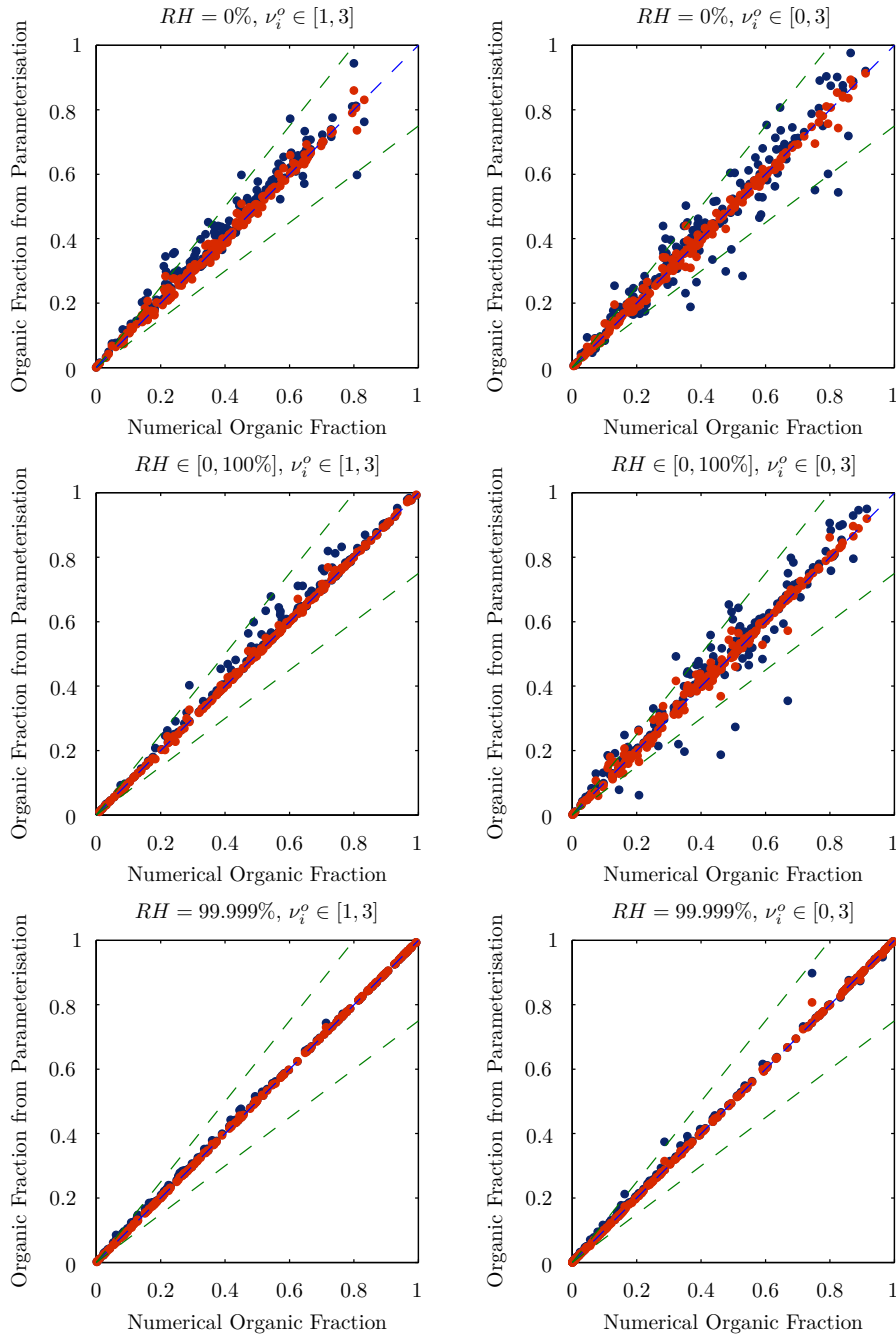
Figure 7. Same as Figure 5 with the addition of the perturbation solution shown in red.

calculated using equilibrium partitioning theory. We have, additionally, simulated two different scenarios designed to study how equilibrium absorptive partitioning theory may perform in large-scale models and the results appear in the supplementary material.

 6.1 Multiple monodisperse aerosol modes

In this section we confirm that the dynamic model converges on the numerical solution from the equilibrium absorptive partitioning theory for multiple monodisperse modes. This allows us to confirm that the errors encountered in Section 6.2 and Section S3 of the supplementary material are not the result of inaccuracies in the standard equilibrium absorptive partitioning theory presented earlier in the paper.

A dynamic parcel model with binned microphysics by Topping et al. (2013) is modified to maintain constant temperature, pressure and water vapour mass; the former two set to 293.15 K and 95000 Pa respectively and the latter is calculated from the specified relative humidity. In the simulations the time taken for small particles to grow to equilibrium is on the order of hundreds of seconds whereas larger particles take thousands. The large particles, however, should take up more of the condensed concentration of the organic compounds due to their higher value of C_T. As a consequence, the vapour phase equilibrates with the total condensed concentration very quickly but the condensed mass on smaller particles exceeds equilibrium and consequently deceeds equilibrium on the larger particles. Once the bulk system reaches equilibrium the large particles can only grow at the same rate that the small particles shrink and this process can take millions of seconds of simulation time to correct to a high degree of accuracy. For the purposes of confirming convergence of the dynamic model towards the solution from equilibrium absorptive partitioning theory it is important to ensure that the dynamic model has converged on an equilibrium to a high degree of accuracy. This solution can then be compared against the equilibrium absorptive partitioning solution to confirm that the two agree.

To obtain accurate convergence of the dynamic model without excessively long simulation times we start the dynamic model from a perturbed equilibrium state in which the condensed mass on each mode deceeds equilibrium by a small amount. The dynamic model is initiated with the remaining organic mass in the vapour phase. Details of how we calculate the initial condensed masses are given in the supplementary material.

Table 3. Material parameters used in the dynamic model simulations. Total SVOC concentrations are 0.47 μg m^{-3} which represents a rescaling of the volatility distribution given in Table 2 by a factor of 0.25.

parameter	ρ_i^o (kg m^{-3})	ρ_j (kg m^{-3})	M_j (kg mol^{-1})	M_i^o (kg mol^{-1})	ν_i^o	ν_j
value	1770	1500	0.132	0.2	3	1

The simulations are run with the material properties given in Table 3 and the size distribution parameters given in Table 4. Figure 9 compares the condensed concentrations for a range of values of the diameter of the first mode; values are denoted above each plot. In each plot the relative humidity was 50%. The top of the red sections of each bar depict the total condensed concentration in each

Table 4. Range of values assigned to the number concentration, N_i, and involatile particle diameter, D_i, used in the dynamic model simulations.

parameter	N_i (cm^{-3})	D_i (nm)
mode 1	100-1000	25-100
mode 2	50	125

475   volatility bin from the dynamic model and the equivalent quantity from the partitioning theory is shown by the black crosses; the two agree almost exactly for all particle sizes shown. The proportions that are condensed on the first and second mode are shown by the area that is coloured green and red, respectively. The height of the green bar shows the condensed concentrations on the first mode from the dynamic model and, as expected, an increase in diameter of these particles results in both an
480   increase in total condensed concentration and the proportion of which is on the first mode. The small particles of diameter 25 nm in the top left plot only account for a small proportion of the condensed concentration, as shown by the small area of green compared to the large area of red. When the size of these particles is increased to 100 nm they take up almost all of the organic material in the condensed phase; the lower right bars have a much larger area of green than red. The analogous
485   quantities from the partitioning theory are shown by the dashed yellow lines which coincide with the tops of the green bars to a high degree of accuracy. The condensed concentrations on the second mode are shown by the height of the red sections of the bars which, when measured from the x axis, are shown by the horizontal black dashed lines across each bar. These too agree exceptionally well with the pink dashed lines, which are the equivalent values from the partitioning theory.

490   Similar plots are shown in Figure 10 but this time the size of the first mode is fixed at 50 nm and the number concentration is varied instead; the values used are shown above each plot. As previously seen, the equilibrium partitioning theory agrees incredibly well with the dynamic model simulations across the parameter space explored. Interestingly, in these plots the total condensed concentration does not increase significantly when the number concentration of the first mode is increased from 100
495   cm^{-3} to 750 cm^{-3}. The proportion on each of the two modes, however, does increase, with almost equal amounts placed on each of the two modes when the first mode has a number concentration of 750 cm^{-3}.

6.2   Application to lognormally distributed particle sizes

Aerosol in the atmosphere is often characterised by multiple polydisperse modes with particles in
500   each mode composed of the same chemical composition. The sizes of particles in each mode are described by size distributions which are a convenient way of treating a polydisperse aerosol as each size distribution can be considered as a single entity.

A common assumption is that the diameters of the particles, D, are lognormally distributed so that the number of aerosol particles, N, per logarithmic size interval is given by

$$\frac{dN}{d\ln D} = \frac{N}{\sqrt{2\pi}\ln\sigma}\exp\left[-\left(\frac{\ln\left(\frac{D}{D_m}\right)}{\sqrt{2}\ln\sigma}\right)^2\right]. \tag{33}$$

505

Here N is the total number of particles and D_m and $\ln\sigma$ are the median diameter and geometric standard deviation. Multiple lognormal size distributions can be added together to form more diverse aerosols

$$\frac{dN}{d\ln D} = \sum_i \frac{N_i}{\sqrt{2\pi}\ln\sigma_i}\exp\left[-\left(\frac{\ln\left(\frac{D}{D_{m,i}}\right)}{\sqrt{2}\ln\sigma_i}\right)^2\right], \tag{34}$$

510 where $D_{m,i}$ and $\ln\sigma_i$ are the median diameter and geometric standard deviation of the ith mode.

The difficulty with applying equilibrium partitioning theory to size distributions is that particles of different sizes have different Kelvin factors and the semi-volatile organic compounds will consequently partition non-uniformly across the sizes of particles. We replace the Kelvin factors by effective values calculated using the median diameters of each mode including the additional con-

515 densed mass of SVOCs. For the equilibrium comparisons used in this section, we assume that the non-volatile compound is represented by lognormal size distributions of particles. After adding the additional condensed mass of SVOCs calculated using equilibrium absorptive partitioning, we assume that the particle sizes are also represented by lognormal size distributions. We use the same geometric standard deviation, $\ln\sigma_i$, as the non-volatile aerosol modes and assume that the median

520 diameter of each mode increases in order to account for the additional aerosol mass from the SVOCs. In Section S4 of the supplementary material, we investigate whether, in practice, the geometric standard deviation can be assumed to remain constant while undergoing condensation of SVOCs.

Table 5. Parameter values used in the first set of dynamic model simulations.

parameter	N (cm^{-3})	D_m (nm)	$\ln\sigma$
mode 1	200	25	0.5
mode 2	50	125	0.1

We begin by comparing the limiting behaviour of the dynamic model against the equilibrium absorptive partitioning theory, presented in this paper, when each mode is represented by a lognor-

525 mal size distribution. In order to isolate the errors resulting from the lognormal size distribution approximation in the equilibrium absorptive partitioning theory from errors in the convergence of the dynamic model, we again start the simulations from a perturbed equilibrium condensed mass. Details of how we derive this initial condensed mass are given in Section 2 of the supplementary material. Further investigations into the applicability of the assumption of equilibrium in more realistic

530 scenarios and time-scales appears in the supplementary material.

The equilibrium calculated using the dynamic model is compared against the equilibrium absorptive partitioning theory in Figure 11 for a range of relative humidities. Lognormal size distributions are defined by the parameters in Table 5 with the material properties in Table 3. Total condensed concentrations from the partitioning theory are shown by the crosses, which lie almost exactly at the top of the red sections which mark the analogous quantity from the dynamic model at equilibrium. The partitioning theory under predicts the condensed concentrations on the first mode (dashed yellow line) compared to the dynamic model (green bar) and the converse is true for the larger mode (dashed pink line and dashed black lines). This is a consequence of the equilibrium absorptive partitioning theory calculating the same total condensed concentration as the dynamic model. The condensed concentration on the larger mode is overpredicted by the equilibrium absorptive partitioning theory and consequently the condensed mass on the smaller mode is underpredicted by the same amount. Due to the condensed masses on the smaller mode being an order of magnitude less than the larger mode this error results in a much larger relative error of between 35% and 50% on the smaller mode. The effect of the increased relative humidity is to increase the total condensed concentration of organics; all of the SVOCs in the five lowest volatility bins are in the condensed phase even at $RH = 0\%$ and so this extra organic mass must come from the higher volatility bins. This is seen by the larger red and green regions for the higher volatility bins in the lower right plot.

The proposed reason for the discrepancies in the condensed masses on the smaller mode is the effect of the Kelvin factor. The Kelvin factor is most variable for smaller diameters and so using an effective value for all particles within a lognormal mode with small median diameter results in appreciable errors. To demonstrate this theory we have carried out further simulations with a smaller mode with median diameter of 50 nm. These are shown in Figure 12 for relative humidities of 0% and 90%. As can be seen, the errors in condensed mass on the smaller mode are eradicated and the two equilibrium solutions are in perfect agreement. We conclude, therefore, that equilibrium partitioning can very accurately calculate the equilibrium condensed mass on lognormal modes if the median diameter is above about 50 nm. In some situations it may be deemed sufficiently accurate to use equilibrium partitioning with lognormal size distributions at smaller diameters, especially when off-set against the reduction in computational complexity compared to solving the dynamic condensation process.

7 Conclusions

This paper presents both a model and an efficient and accurate parameterisation of the solution that is suitable for investigations in a wide range of research areas that use equilibrium absorptive partitioning theory. Of particular interest to the authors is cloud droplet activation parameterisations and, ultimately, inclusion in global climate models.

565   The model itself predicts the equilibrium condensed concentrations of organics onto multiple monodisperse aerosol modes incredibly accurately compared to the equilibrium solution from a dynamic model. This holds true for a range of particle sizes, number concentrations and relative humidities.

The proposed parameterisation is found to be exceptionally accurate for a wide range of param-
570   eters. Assuming the same mole fraction for all of the modes offers a quick method of obtaining a reasonably accurate approximation for all but the smallest van't Hoff factors of the involatile compounds, but performs well at high values of relative humidity. The perturbation correction term offers significant improvements at lower relative humidity, especially for smaller van't Hoff factors, with negligible increase in computational expense.

575   The condensed mass calculated using equilibrium absorptive partitioning theory with lognormal size distributions of involatile particles agrees very well with the limiting behaviour of the dynamic model if the median diameters of the modes are above 50 nm. Below this size the Kelvin term becomes important and results in non-negligible errors. This is further corroborated in the more realistic scenarios simulated in the supplementary material.

580   ## 8   Code Availability

All Matlab source code used in the generation of the plots in this paper, including a solver for the multiple mode equilibrium partitioning theory equations, is available at dx.doi.org/10.5281/zenodo.34025.

Appendix A

The implicit equations governing the leading order solution can be manipulated to give an explicit
585   expression for each of the condensed concentrations, $\bar{C}_{ij}$, in terms of the average mole fraction. We present the algebra for such a step here. The coupled equations are given by (29) and are restated here

$$
\bar{C}_{ij}^c \;=\; \frac{C_j - \displaystyle\sum_r \bar{C}_{rj}^c + \bar{C}_{ij}^c}{1 + \dfrac{C_j^*/\eta_i}{C_i^o(1+\beta)}}.
$$

We can make use of the notation given by (14) to write the summation term as $\bar{C}_j^c$ and rearrange the
590   denominator on the right-hand side to give

$$
\bar{C}_{ij}^c \;=\; \left(C_j - \bar{C}_j^c + \bar{C}_{ij}^c\right)\frac{C_i^o(1+\beta)}{C_i^o(1+\beta) + C_j^*/\eta_i}.
$$

The explicit dependence on $\bar{C}_{ij}^c$ can be factorised onto the left-hand side

$$
\left(\frac{C_j^*/\eta_i}{C_i^o(1+\beta) + C_j^*/\eta_i}\right)\bar{C}_{ij}^c \;=\; \frac{C_i^o(1+\beta)\left(C_j - \bar{C}_j^c\right)}{C_i^o(1+\beta) + C_j^*/\eta_i},
$$

which further reduces to

$$\bar{C}_{ij}^c \quad = \quad \frac{C_i^o(1+\beta)\left(C_j - \bar{C}_j^c\right)}{C_j^*/\eta_i}. \tag{A1}$$

By summing over i an equation for C_j^c is obtained

$$\bar{C}_j^c \quad = \quad \left(C_j - \bar{C}_j^c\right) \sum_r \frac{C_r^o(1+\beta)}{C_j^*/\eta_r},$$

which has the solution

$$\bar{C}_j^c = \phi_j C_j,$$

where ϕ_j depends on β and η_i and is given by

$$\phi_j(\beta,\eta_i) \quad = \quad \frac{\displaystyle\sum_r \frac{C_r^o(1+\beta)}{C_j^*/\eta_r}}{1 + \displaystyle\sum_r \frac{C_r^o(1+\beta)}{C_j^*/\eta_r}}, \tag{A2}$$

The individual condensed concentrations are then be calculated using (A1) which can now be written as

$$\bar{C}_{ij}^c \quad = \quad \frac{C_i^o(1+\beta)\left(1-\phi_j\right)C_j}{C_j^*/\eta_i}.$$

Appendix B

The details of the linearisation of the perturbation equations (31) are presented in this appendix and we begin by restating the set of non-linear equations

$$\bar{C}_{ij}^c + \hat{C}_{ij}^c = \frac{C_j - \displaystyle\sum_r \bar{C}_{rj}^c + \bar{C}_{ij}^c - \displaystyle\sum_r \hat{C}_{rj}^c + \hat{C}_{ij}^c}{1 + \dfrac{C_j^* \bar{K}_{ij}/\bar{\eta}_i}{C_i^o + \displaystyle\sum_k \bar{C}_{ik}^c + \displaystyle\sum_k \hat{C}_{ik}^c}}.$$

The denominator on the right-hand side can be rearranged to give

$$
610 \quad \bar{C}_{ij}^c + \hat{C}_{ij}^c = \left(C_j - \sum_r \bar{C}_{rj}^c + \bar{C}_{ij}^c - \sum_r \hat{C}_{rj}^c + \hat{C}_{ij}^c \right) \left(\frac{C_i^o + \sum_k \bar{C}_{ik}^c + \sum_k \hat{C}_{ik}^c}{C_i^o + \sum_k \bar{C}_{ik}^c + \sum_k \hat{C}_{ik}^c + C_j^* \bar{K}_{ij}/\bar{\eta}_i} \right)
$$

$$
= \left(\frac{C_j - \sum_r \bar{C}_{rj}^c + \bar{C}_{ij}^c - \sum_r \hat{C}_{rj}^c + \hat{C}_{ij}^c}{C_i^o + \sum_k \bar{C}_{ik}^c + C_j^* \bar{K}_{ij}/\bar{\eta}_i} \right) \left(\frac{C_i^o + \sum_k \bar{C}_{ik}^c + \sum_k \hat{C}_{ik}^c}{1 + \dfrac{\sum_k \hat{C}_{ik}^c}{C_i^o + \sum_k \bar{C}_{ik}^c + C_j^* \bar{K}_{ij}/\bar{\eta}_i}} \right)
$$

$$
= \left(\frac{C_j - \sum_r \bar{C}_{rj}^c + \bar{C}_{ij}^c - \sum_r \hat{C}_{rj}^c + \hat{C}_{ij}^c}{C_i^o + \sum_k \bar{C}_{ik}^c + C_j^* \bar{K}_{ij}/\bar{\eta}_i} \right) \left(C_i^o + \sum_k \bar{C}_{ik}^c + \sum_k \hat{C}_{ik}^c \right)
$$

$$
\times \left(1 + \frac{\sum_k \hat{C}_{ik}^c}{C_i^o + \sum_k \bar{C}_{ik}^c + C_j^* \bar{K}_{ij}/\bar{\eta}_i} \right)^{-1}.
$$

We now assume that the perturbations are sufficiently small that

$$
615 \quad \left| \frac{\sum_k \hat{C}_{ik}^c}{C_i^o + \sum_k \bar{C}_{ik}^c + C_j^* \bar{K}_{ij}/\bar{\eta}_i} \right| \ll 1, \tag{B1}
$$

so that the third term on the right-hand side can be approximated by its Taylor series expansion of the form

$$
\frac{1}{1+x} \approx 1 - x + O(x^2),
$$

with x equal to the term (B1),

$$
620 \quad \bar{C}_{ij}^c + \hat{C}_{ij}^c = \left(\frac{C_j - \sum_r \bar{C}_{rj}^c + \bar{C}_{ij}^c - \sum_r \hat{C}_{rj}^c + \hat{C}_{ij}^c}{C_i^o + \sum_k \bar{C}_{ik}^c + C_j^* \bar{K}_{ij}/\bar{\eta}_i} \right) \left(C_i^o + \sum_k \bar{C}_{ik}^c + \sum_k \hat{C}_{ik}^c \right)
$$

$$
\times \left(1 - \frac{\sum_k \hat{C}_{ik}^c}{C_i^o + \sum_k \bar{C}_{ik}^c + C_j^* \bar{K}_{ij}/\bar{\eta}_i} + O\left(\left[\hat{C}_{ij}^c \right]^2 \right) \right).
$$

The right-hand side can be linearised assuming the terms of order $O\left(\left[\hat{C}_{ij}^c\right]^2\right)$ are negligible.

$$\bar{C}_{ij}^c + \hat{C}_{ij}^c = \cfrac{C_j - \sum\limits_r \bar{C}_{rj}^c + \bar{C}_{ij}^c}{1 + \cfrac{C_j^* \bar{K}_{ij}/\bar{\eta}_i}{C_i^o + \sum\limits_k \bar{C}_{ik}^c}} + \cfrac{-\sum\limits_r \hat{C}_{rj}^c + \hat{C}_{ij}^c}{1 + \cfrac{C_j^* \bar{K}_{ij}/\bar{\eta}_i}{C_i^o + \sum\limits_k \bar{C}_{ik}^c}}$$

$$+ \left(\cfrac{C_j - \sum\limits_r \bar{C}_{rj}^c + \bar{C}_{ij}^c}{C_i^o + \sum\limits_k \bar{C}_{ik}^c + C_j^* \bar{K}_{ij}/\bar{\eta}_i}\right) \sum\limits_k \hat{C}_{ik}^c$$

$$- \cfrac{\left(C_j - \sum\limits_r \bar{C}_{rj}^c + \bar{C}_{ij}^c\right)\left(C_i^o + \sum\limits_k \bar{C}_{ik}^c\right)}{\left(C_i^o + \sum\limits_k \bar{C}_{ik}^c + \cfrac{C_j^* \bar{K}_{ij}}{\bar{\eta}_i}\right)^2} \sum\limits_k \hat{C}_{ik}^c.$$

We can factorise this to give

$$\hat{C}_{ij}^c + \cfrac{\sum\limits_r \hat{C}_{rj}^c - \hat{C}_{ij}^c}{1 + \cfrac{C_j^* \bar{K}_{ij}/\bar{\eta}_i}{C_i^o + \sum\limits_k \bar{C}_{ik}^c}} - \left[\cfrac{\left(C_j - \sum\limits_r \bar{C}_{rj}^c + \bar{C}_{ij}^c\right)\left(C_i^o + \sum\limits_k \bar{C}_{ik}^c\right)\cfrac{C_j^* \bar{K}_{ij}}{\bar{\eta}_i}}{\left(C_i^o + \sum\limits_k \bar{C}_{ik}^c + \cfrac{C_j^* \bar{K}_{ij}}{\bar{\eta}_i}\right)^2}\right] \sum\limits_k \hat{C}_{ik}^c$$

$$= \cfrac{C_j - \sum\limits_r \bar{C}_{rj}^c + \bar{C}_{ij}^c}{1 + \cfrac{C_j^* \bar{K}_{ij}/\bar{\eta}_i}{C_i^o + \sum\limits_k \bar{C}_{ik}^c}} - \bar{C}_{ij}^c.$$

By denoting the coefficient in the square brackets by $\mathcal{L}_{ij}$ together with

$$\bar{\xi}_{ij} = \left(1 + \cfrac{C_j^* \bar{K}_{ij}/\bar{\eta}_i}{C_i^o + \sum\limits_k \bar{C}_{ik}^c}\right)^{-1}, \tag{B2}$$

this expression can be made more notationally simplistic

$$\left(1 - \bar{\xi}_{ij}\right)\hat{C}_{ij}^c + \bar{\xi}_{ij} \sum\limits_r \hat{C}_{rk}^c - \mathcal{L}_{ij} \sum\limits_k \hat{C}_{ij}^c = \cfrac{C_j - \sum\limits_r \bar{C}_{rj}^c + \bar{C}_{ij}^c}{1 + \cfrac{C_j^* \bar{K}_{ij}/\bar{\eta}_i}{C_i^o + \sum\limits_k \bar{C}_{ik}^c}} - \bar{C}_{ij}^c.$$

It is important to note that both $\bar{\xi}_{ij}$ and $\mathcal{L}_{ij}$ depend on the leading order solution but are independent of the perturbation, $\hat{C}_{ij}$, and as such this equation is now linear in these quantities.

635 *Acknowledgements.* The research leading to these results has received funding from the European Union's Seventh Framework Programme (FP7/2007-2013) under grant agreement number 603445.

References

Albrecht, B. A.: Aerosols, cloud microphysics and fractional cloudiness, Science, 245, 1227–1230, 1989.

Andreae, M. O. and Crutzen, P. J.: Atmospheric aerosols: biogeochemical sources and role in atmospheric chemistry, Science, 276, 1052–1058, 1997.

Barley, M., Topping, D. O., Jenkin, M. E., and McFiggans, G.: Sensitivities of the absorptive partitioning model of secondary organic aerosol formation to the inclusion of water, Atmospheric Chemistry and Phyics, 9, 2919–2932, 2009.

Biniecka, M. and Caroli, S.: Analytic methods for the quantification of volatile aromatic compounds, Trends in Analytic Chemistry, 30, 2011.

Borbon, A., Gilman, J., Kuster, W., Grand, N., Chevaillier, S., Colomb, A., Dolgorouky, C., Gros, V., Lopez, M., Sarda-Esteve, R., Holloway, J., Stutz, J., Petetin, H., McKeen, S., Beekmann, M., Warneke, C., Parrish, D., and de Gouw, J.: Emission ratios of anthropogenic volatile organic compounds in northern mid-latitude megacities: Observations versus emission inventories in Los Angeles and Paris, Journal of Geophysical Research, 118, 2041 – 2057, 2013.

Cai, X. an Griffin, R. J.: Theoretical modeling of the size-dependent influence of surface tension in the absorptive partitioning of semi-volatile organic compounds, Journal of Atmospheric Chemistry, 50, 139–158, 2005.

Cappa, C. D. and Jimenez, J. L.: Quatitative estimates of the volatility of ambient organic aerosol, Atmospheric Chemistry and Phyics, 10, 5409–5424, 2010.

Cappa, C. D. and Wilson, K. R.: Evolution of organic aerosol mass spectra upon heating: implications for OA phase and partitioning behaviour, Atmos. Chem. Phys, 11, 1895 – 1911, 2011.

Chýlek, P. and Coakley Jr, J. A.: Aerosols and climate, Science, pp. 75–77, 1974.

de Roos, K.: Effect of texture and microstructure on flavour retention and release, International Dairy Journal, 13, 593–605, 2003.

Donahue, N. M., Robinson, A. L., Stanier, C. O., and Pandis, S. N.: Coupled partitioning, dilution and chemical aging of semivolatile organics, Environmental Science and Technology, 40, 2635–2643, 2006.

Dusek, U., Frank, G. P., Hildebrandt, L., Curtius, J., Schneider, J., Walter, S., Chand, D., Drewnick, F., Hings, S., Jung, D., Borrman, S., and Andreae, M. O.: Size matters more than chemistry for cloud-nucleating ability of aerosol particles, Science, 312, 1375–1378, 2006.

Ehn, M., Thornton, J., Kleist, E., Sipilä, M., Junninen, H., Pullinen, I., Springer, M., Rubach, F., Tillmann, R., Lee, B., Lopez-Hilfiker, F., Andres, S., Acir, I., Rissanen, M., Jokinen, T., Schobesberger, S., Kangasluoma, J., Kontkanen, J., Nieminen, T., Kurtén, T., Nielsen, L., Jørgensen, S., Kjaergaard, H., Canagaratna, M., Maso, M., Berndt, T., Petäjä, T., Wahner, A., Kerminen, V., Kulmala, M., Worsnop, D., Wildt, J., and Mentel, T.: A large source of low-volatility secondary organic aerosol, Nature, 506, 476 – 479, 2014.

Epstein, S. and Gibson, A.: Avoidable Causes of Childhood Cancer, Xlibris, 2013.

Forster, P., Ramaswamy, V., Artaxo, P., Berntsen, T., Betts, R., Fahey, D. W., Haywood, J., Lean, J., Lowe, D. C., Myhre, G., Nganga, J., Prinn, R. G., Schulz, M., Van Dorland, R., and Van Dorland, R.: Changes in Atmospheric Constituents and in Radiative Forcing Chapter 2., Cambridge University Press, 2007.

Ghan, S. J., Guzman, G., and Abdul-Razzak, H.: Competition Between Sea Salt and Sulphate Particles as Cloud Condensation Nuclei, Journal of the Atmospheric Sciences, 55, 3340–3347, 1998.

Goldstein, A. H. and Galbally, I. E.: Known and unexplored organic constituents in the earth's atmosphere, Environmental Science and Technology, 41, 1514–1521, 2007.

Gray, H. A., Cass, G. R., Huntzicker, J. J., Heyerdahl, E. K., and Rau, J. A.: Characteristics of atmospheric or-
680   ganic and elemental carbon particle concentrations in Los Angeles, Environmental Science and Technology, 20, 580–589, 1986.

Hallquist, M., Wenger, J. C., Baltensperger, U., Rudich, Y., Simpson, D., Claeys, M., Dommen, J., Donahue, N. M., George, C., Goldstein, A. H., Hamilton, J. F., Herrmann, H., Hoffmann, T., Linuma, Y., Jang, M., Jenkin, M. E., Jimenez, J. L., Kiender-Scharr, A., Maenhaut, W., McFiggans, G., Mentel, T. F., Monod, A.,
685   Preévôt, A. S. H., Seinfeld, J. H., Surratt, J. D., Szmigielski, R., and Wildt, J.: The formation, properties and impact of secondary organic aerosol: current and emerging issues, Atmospheric Chemistry and Phyics, 9, 5155–5236, 2009.

Hui, Y., Chen, F., Nollet, L., Guine, R., Martin-Belloso, O., Minguez-Mosquera, M., Paliyath, G., Pessoa, F., Le Quéré, J., Sidhu, J., Sinha, N., and Stanfield, P.: Handbook of Fruit and Vegetable Flavors, Wiley-
690   Blackwell, 1 edn., 2010.

Jimenez, J. L. and et. al.: Evolution of organic aerosols in the atmosphere, Science, 326, 1525–1529, 2009.

Klein, R.: Get a Whiff of This, The New Republic, 212, 1995.

Lohmann, U., Feicher, J., Penner, J., and Leaitch, R.: Indirect effect of sulphate and carbonaceous aerosols: a mechanistic treatment, Journal of Geophysical Research, 105, 12 193–12 206, 2000.

695   McCormick, R. A. and Ludwig, J. H.: Climate modification by atmospheric aerosols, Science, 156, 1358–1359, 1967.

Mendes, B., Gonçalves, J., and Câmara, J.: Effectivesness of high-throughput miniaturized sorbent- and solid phase microextraction techniques combined with gas chromatography-mass spectrometry analysis for a rapid screening of volatile and semi-volatile composition of wines- a comparative study, Talanta, 88, 79–94, 2012.

700   Morgan, W. T., Allan, J. D., Bower, K. N., Esselborn, M., Harris, B., Henzing, J. S., Highwood, E. J., Kiender-Scharr, A., McMeeking, G. R., Mensah, A. A., Northway, M. J., Osborne, S., Williams, P. I., Krejci, R., and Coe, H.: Enhancement of the aerosol direct radiative effect by semi-volatile aerosol components: airborne measurements in North-Western Europe, Atmospheric Chemistry and Phyics, 10, 8151–8171, 2010.

Morris, E.: Fragrance: the story of perfume from Cleopatra to Chanel, Scriber, 1984.

705   O'Donnell, D., Tsigaridis, K., and Feichter, J.: Estimating the direct and indirect effects of secondary organic aerosols using ECHAM5-HAM, Atmos. Chem. Phys, 11, 8635 – 8659, 2011.

Odum, J. R., Hoffmann, T., Bowman, F., Collins, D., Flagan, R. C., and Seinfeld, J. H.: Gas/particle partitioning and secondary organic aerosol yields, Environmental Science and Technology, 30, 2580–2585, 1996.

Pankow, J. F.: An absorptive model of gas/particle partitioning of organic compounds in the atmosphere, Atmo-
710   spheric Environment, 28, 185–188, 1994.

Pruppacher, H. R. and Klett, J. D.: Microphysics of Clouds and Precipitation, Springer, 2nd edn., 1977.

Rogers, R. and Yau, M. K.: A short course in cloud physics, Butterworth-Heinemann, third edn., 1996.

Simpson, D., Benedictow, A., Berge, H., Bergstroöm, R., Emberson, L., Fagerli, H., Flechard, C., Hayman, G., Gauss, M., Jonson, J., Jenkin, M., Nyiri, A., Richter, C., Semeena, V., Tsyro, S., Tuovinen, J., Valdebenito,
715   A., and Wind, P.: The EMEP MSC-W chemical transport model - technical description, Atmos. Chem. Phys, 12, 7825 – 7865, 2012.

Sitaramaraju, Y., van Hul, A., Wolfs, K., van Schepdael, A., Hoogmartens, J., and Adams, E.: Static headspace gas chromatography of (semi-)volatile drugs in pharmaceuticals for topical use, Journal of Pharmaceutical and Biomedical Analysis, 47, 834–840, 2008.

720 Smith, G., Woods, E., Baer, T., and Miller, R.: Aerosol Uptake described by numerical solution of the diffusion-reaction equations in the particle, J. Phys. Chem., 107, 9582 – 9587, 2003.

Stevens, B. and Feingold, G.: Untangling aerosol effects on clouds and precipitation in a buffered system, Nature, 461, 607–613, 2009.

Topping, D., Connolly, P., and McFiggans, G.: Cloud droplet number enhanced by co-condensation of organic

725 vapours, Nature Geoscience, 6, 443–446, 2013.

Topping, D. O. and McFiggans, G.: Tight coupling of particle size, number and composition in atmospheric cloud droplet activation, Atmospheric Chemistry and Phyics, 12, 3253–3260, 2012.

Tsimpidi, A. P., Karydis, V. A., Pozzer, A., Pandis, and Lelieveld, J.: ORACLE (v1.0): modeule to simulate the organic aerosol composition and evolution in the atmosphere, Geosci. Model Dev., 7, 3153 – 3172, 2014.

730 Twomey, S.: The nuclei of natural cloud formation part II: the supersaturation in natural clouds and the variation of cloud droplet concentration, Pure and Applied Geophysics, 43, 243–249, 1959.

Twomey, S.: Pollution and the planetary albedo, Atmospheric Science, 8, 1251–1256, 1974.

Twomey, S.: The influence of pollution on the shortwave albedo of clouds, Journal of the Atmospheric Sciences, 34, 1149–1152, 1977.

735 Vaden, T., Imre, D., Ber'anek, J., Shrivastava, M., and Zelenyuk, A.: Evaporation kinetics and phase of laboratory and ambient secondary organic aerosol, PNAS, 108, 2011.

Vernocchi, P., Ndagijimana, M., Serrazanetti, D., Gianotti, A., Vallicelli, M., and Guerzoni, M.: Influence of starch addition and dough microstructure on fermentation aroma production by yeasts and lactobacilli, Food Chemistry, 108, 1217–1225, 2008.

740 Wang, J., MacNeil, J., and Kay, J.: Chemical Analysis of Antibiotic Residues in Food, Wiley, 2011.

Wu, B., Zhang, X., Zhang, X., Yasun, A., Zhang, Y., Zhao, D., Ford, T., and Cheng, S.: Semi-volatile organic compounds and trace elements in the Yangtze River source of drinking water, Ecotoxicology, 18, 707–714, 2009.

Yu, F.: A secondary organics aerosol formulation model considering successive oxidation aging and kinetic con-

745 densation of organic compounds: global scale implications, Atmospheric Chemistry and Phyics, 11, 1083–1099, 2011.

Zarra, T., Naddeo, V., Belgiorno, V., and Reiser, M. Kranert, M.: Instrumental characterization of odour: a combination of offactory and analytical methods, Water Science and Technology, 59, 1603–1609, 2009.

Zhang et. al., Q.: Ubiquity and dominance of oxygenated species in organic aerosols in anthropogenically-

750 influenced Northern Hemisphere midlatitudes, Geophysical Research Letters, 34, 2007.

Zobrist, B., Soonsin, V., Luo, B., Kreiger, U., Marcolli, C., Peter, T., and Koop, T.: Ultra-slow water diffusion in aqueous sucrose glasses, Physical Chemistry Chemical Physics, 13, 3514 – 3526, 2011.
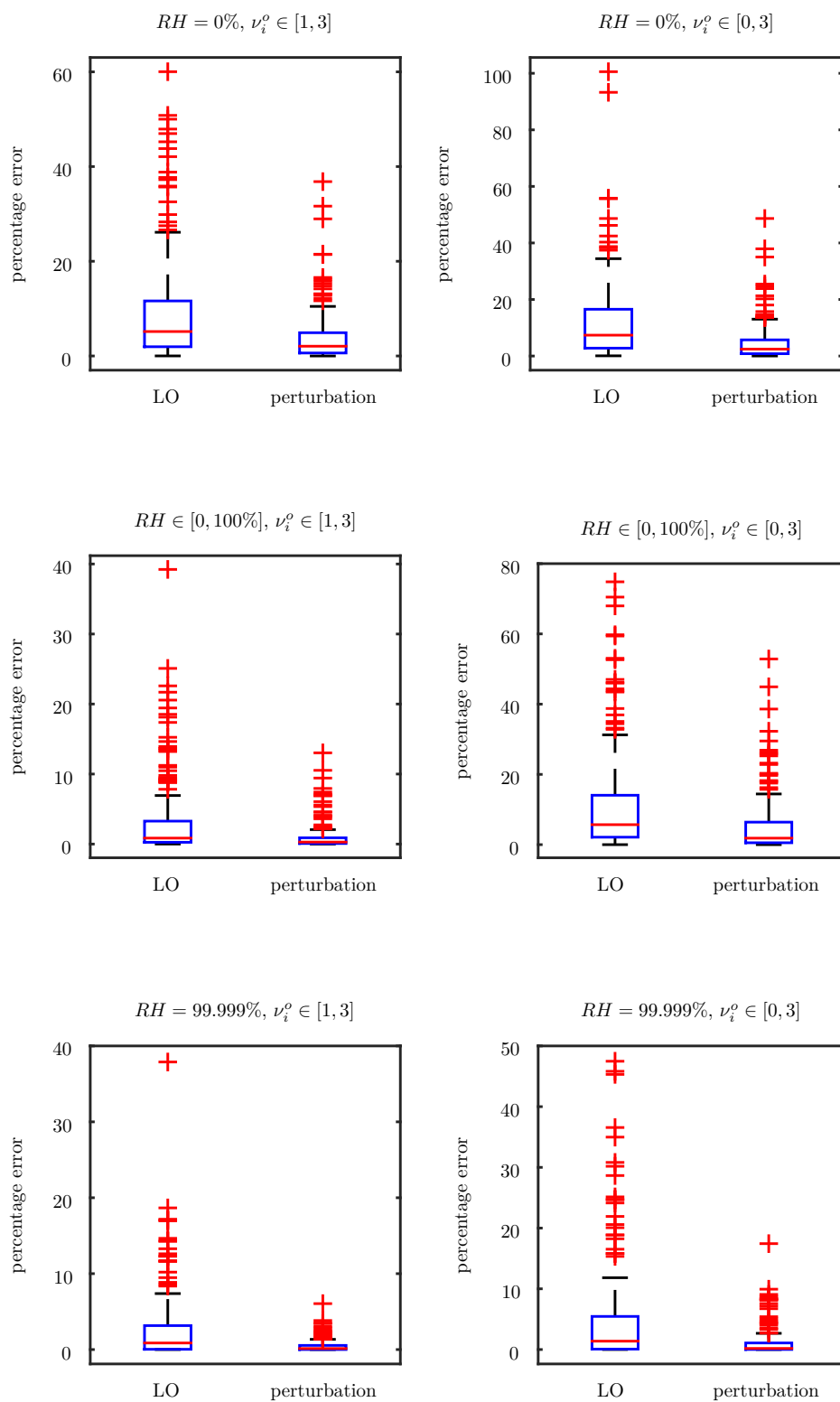
Figure 8. Comparison of the percentage errors in organic mass fraction from the two approximations in relation to those calculated using the non-linear solver for the data points in Figure 7. The leading order (LO) and perturbation solutions are shown by the left and right box and whisker plots in each figure, respectively.
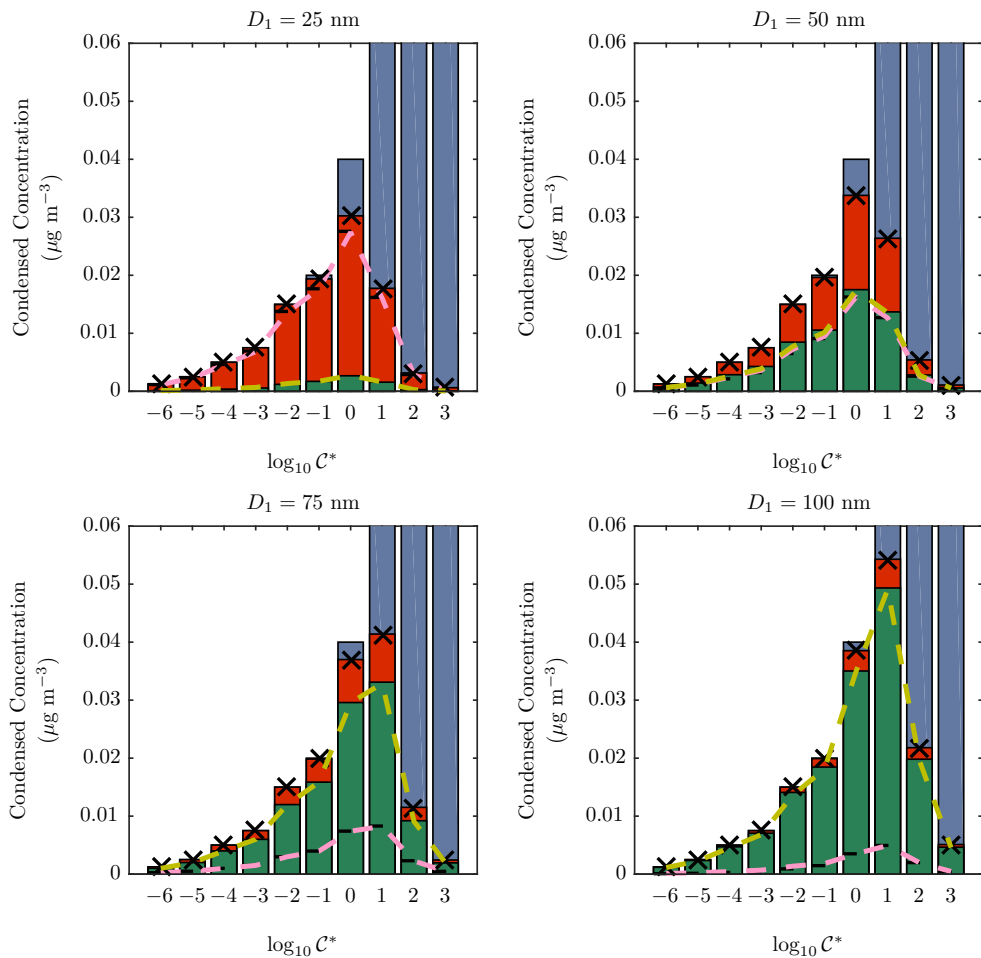
Figure 9. Stacked bar charts showing the condensed concentrations from the two models. Each bar shows the total concentration of organics in each volatility bin and are coloured to show the proportion which is in the vapour phase (blue) and the condensed phases on the first and second modes (green and red respectively). The height of the horizontal black dashed lines across each bar marks the condensed concentrations on the second mode only (the height of the red regions as measured from the x axis). Total concentrations in each volatility bin from the partitioning theory are shown by the black crosses and the amount on the first and second modes are shown by the yellow and pink dashed lines respectively. The y axis is cut-off at 0.04 and 0.05 for clarity. The diameter of the first mode is denoted above each plot and the number concentration is 1000 cm^{-3} while the second mode has a median diameter of 125 nm and a number concentration of 50 cm^{-3}.
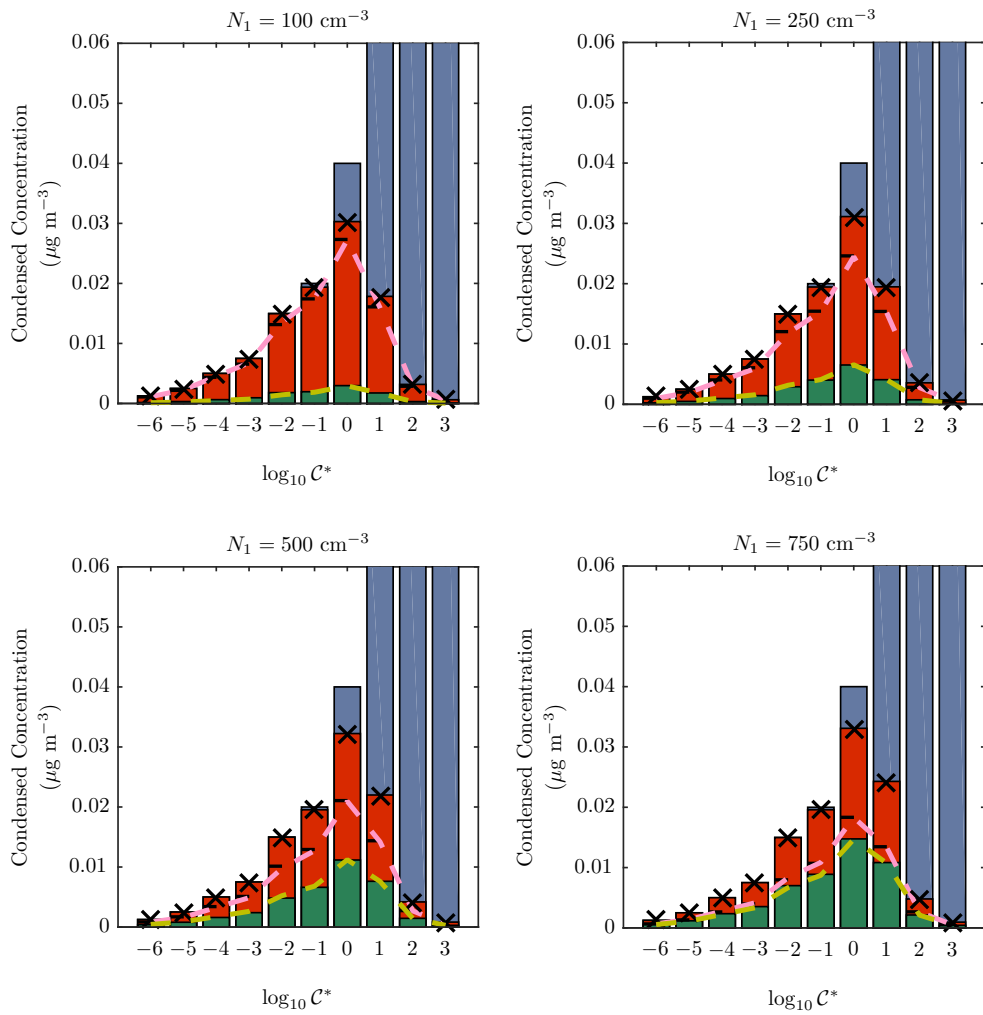
Figure 10. Same as Figure 9 but with differing number concentration of the first mode in each plot and a diameter of 50 nm. The second mode has a median diameter of 125 nm and a number concentration of 50 cm^{-3}.
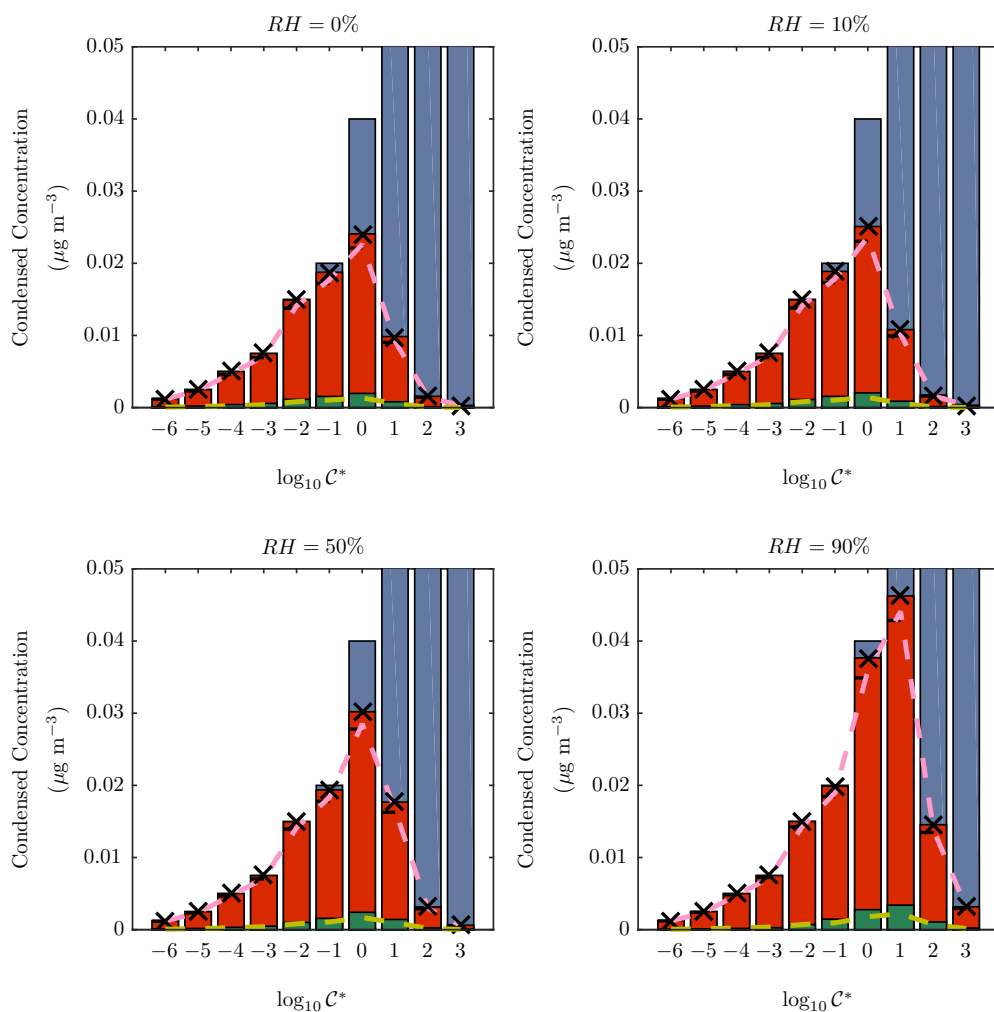
Figure 11. Same as Figure 9 for involatile aerosol modes represented by lognormal size distributions with number concentrations of $200\ cm^{-3}$ and $50\ cm^{-3}$ and median diameters of 25 nm and 125 nm, respectively. The geometric standard deviations are 0.5 and 0.1. The relative humidity used in each simulation is stated above each plot.
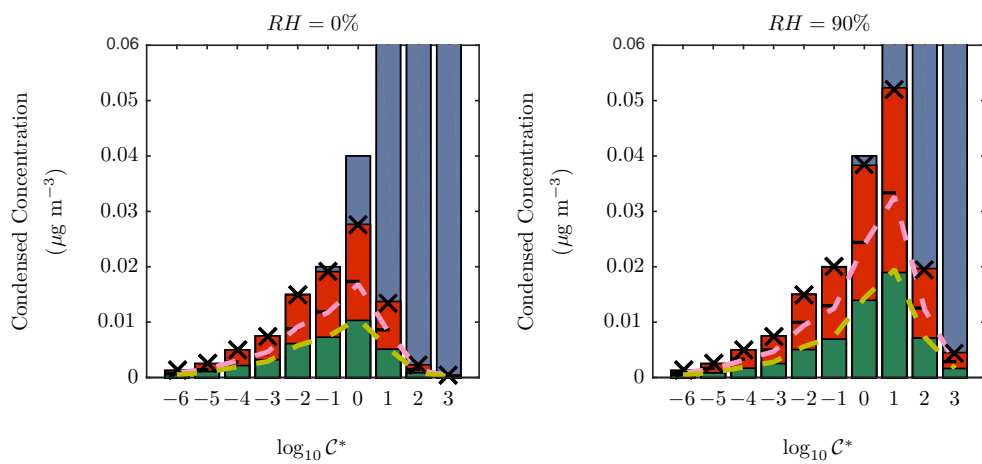
Figure 12. Same as Figure 11 but the first mode has a median diameter of 50 nm and a number concentration of 200 cm^{-3}. The second mode has a median diameter of 125 nm and a number concentration of 50 cm^{-3}. The geometric standard deviations are 0.5 and 0.1.